BNL-210831-2018-JAAM

Insight into the Phase Transformation Pathways of Copper Oxidation: from Oxygen Chemisorption on the Clean Surface to Multi-Layer Bulk Oxide Growth

J. Wang, J. A. Boscoboinik

To be published in "The Journal of Physical Chemistry"

October 2018

Center for Functional Nanomaterials

Brookhaven National Laboratory

U.S. Department of Energy

USDOE Office of Science (SC), Basic Energy Sciences (BES) (SC-22)

Notice: This manuscript has been authored by employees of Brookhaven Science Associates, LLC under Contract No. DE-SC0012704 with the U.S. Department of Energy. The publisher by accepting the manuscript for publication acknowledges that the United States Government retains a non-exclusive, paid-up, irrevocable, world-wide license to publish or reproduce the published form of this manuscript, or allow others to do so, for United States Government purposes.

DISCLAIMER

This report was prepared as an account of work sponsored by an agency of the United States Government. Neither the United States Government nor any agency thereof, nor any of their employees, nor any of their contractors, subcontractors, or their employees, makes any warranty, express or implied, or assumes any legal liability or responsibility for the accuracy, completeness, or any third party's use or the results of such use of any information, apparatus, product, or process disclosed, or represents that its use would not infringe privately owned rights. Reference herein to any specific commercial product, process, or service by trade name, trademark, manufacturer, or otherwise, does not necessarily constitute or imply its endorsement, recommendation, or favoring by the United States Government or any agency thereof or its contractors or subcontractors. The views and opinions of authors expressed herein do not necessarily state or reflect those of the United States Government or any agency thereof.

Insight into the Phase Transformation Pathways of Copper Oxidation: from Oxygen Chemisorption on the Clean Surface to Multi-Layer Bulk Oxide Growth

Jianyu Wang[†], Chaoran Li[†], Yaguang Zhu[†], Jorge Anibal Boscoboinik[‡], Guangwen Zhou[*, †]

[†]Department of Mechanical Engineering & Materials Science and Engineering Program, State University of New York, Binghamton, NY 13902

[‡] Center for Functional Nanomaterials, Brookhaven National Laboratory, Upton, NY 11973

Abstract

We have employed ambient-pressure X-ray photoelectron spectroscopy to monitor the full pathway of copper oxidation from the initial stages of oxygen chemisorption to oxide nucleation and growth and then to growing continuous oxide layer. By increasing oxygen pressure in a stepwise way from $pO_2=10^{-7}$ Torr to 1 Torr at T=350°C, we show that the oxidation of Cu(100) takes place by dissociative chemisorption of oxygen to first form the p(2×2) phase at $pO_2=1\times10^{-7}$ Torr, which then transforms to the $(2\sqrt{2}\times\sqrt{2})R45°$ missing-row reconstruction with a higher oxygen coverage and upon increasing pO_2 from 1×10^{-6} Torr to 1×10^{-3} Torr. After reaching $pO_2=1\times10^{-2}$ Torr, nucleation and growth of Cu_2O islands occurs by consuming the $(2\sqrt{2}\times\sqrt{2})R45°$ regions. Increasing pO_2 to 0.1 Torr results in the continued Cu_2O growth with increased surface roughness. The surface is quickly covered with a CuO layer upon increasing pO_2 to 1 Torr, at which the surface oxidation occurs via the CuO/Cu_2O bilayer growth. The measurements delineate the range of pO_2 required for the crossover between the different stages of the surface oxidation and may have practical importance by tuning the oxidation conditions that allow for controlling the oxide phase and atomic structure of the surface.

*To whom correspondence should be addressed: gzhou@binghamton.edu

1. INTRODUCTION

Surface oxidation of metals is a spontaneous process that induces profound changes in materials properties and functionality ranging from corrosion resistance to the production of important chemicals in heterogeneous catalysis. Fundamentally, the oxidation of metals represents a remarkably complex scenario that involves hierarchical multiple length scales proceeding generally from the atomic-scale oxygen surface chemisorption to the nanoscale oxide nucleation and growth and then to the formation of a continuous, macroscopically thick oxide layer[1,2]. Despite of this general knowledge of the reaction pathway, the atomistic mechanisms governing the crossovers between the different reaction stages leading to the onset, promotion and termination of the bulk oxidation are largely unknown.

Over the past few decades, surface science studies on the oxidation of metal surfaces under idealized conditions, i.e., ultrahigh vacuum (UHV), have provided a wealth of information on the microscopic processes of oxygen chemisorption including adsorption sites and oxygen adsorption induced surface restructuring[3]. The range of oxygen pressure (pO_2) typically accessible in the surface science methods is insufficient for probing bulk oxide formation. In contrast, much attention in the traditional oxidation studies has been devoted to the kinetics of growing continuous oxide films under the ambient pressure conditions. Therefore, an information gap exists between the surface science methods that mainly focus on the oxygen adsorption of up to one monolayer and that of the traditional oxidation studies of bulk oxide growth. A key challenge in bridging this knowledge gap has been the lack of experimental tools capable of monitoring the full reaction pathway by performing measurements of the surface oxidation with pO_2 spanning from the UHV conditions that allow for studying surface oxygen chemisorption with carefully dosing small amounts of oxygen to the high pO_2 regimes required for bulk oxide formation. With the development of new experimental tools with the environmental

capabilities, it is now possible to monitor an oxidation process under the operando conditions. Ambient-pressure x-ray photoelectron spectroscopy (AP-XPS) [4–6] is one of these tools that are capable of monitoring the chemical states and reaction kinetics of gas-surface reactions at the atomic scale in real time and with pO_2 varying from UHV to elevated pressures, namely, the near-ambient condition. In this work, we employ the AP-XPS technique to study the oxidation of Cu(100) over a wide range of pO_2, which allows for monitoring the full reaction pathway from the initial stages of surface oxygen chemisorption to the oxide nucleation and growth and then to the growing continuous oxide layer.

Among many metal-oxygen systems, the oxidation of copper has been a rich source of information to understand the corrosion of metals and functionalities of metal-oxide catalytic systems due to its multiple oxidation states (Cu^{+} and Cu^{2+}) and different crystal structures of the copper oxides (cubic for Cu_2O and monoclinic for CuO[7]). In addition to being a model experimental system, Cu is also of great practical importance because of its wide application in different oxidizing environments, including Cu interconnect technology[8] and Cu based catalysts for catalytic reactions such as fuel cells[9], hydrogen production[10], and emission control[11]. A critical issue for all these applications is related to the oxidation of copper, which can lead to significant changes in surface properties[12]. Copper is a unique system for studying the oxidation pathway. This is, the initial state (e.g., the clean metal surface and several oxygen chemisorption geometries) and the final stable state (e.g., either Cu_2O or CuO) are well identified at the atomic scale. However, the reaction pathway leading to the transition towards a stable oxide is still not clearly elucidated. Upon exposure to oxygen gas, Cu(100) typically goes through two sequential surface reconstructions: for oxygen coverage below 0.3 monolayer (ML), oxygen adsorbs on fourfold hollow sites resulting in a Cu(100)-p(2×2) structure[13]. Increasing oxygen exposure results in the nucleation and growth of the $\left(2\sqrt{2} \times \sqrt{2}\right)R45°$ missing-row (MR) reconstruction[14,15]. Further

oxygen adsorption leads to bulk oxide formation of Cu_2O and CuO, where the oxide growth is attributed to outward diffusion of Cu cations following the parabolic rate law[16].

Concerning the fundamental studies of copper oxidation, some basic questions still exist such as the predominated chemical states (Cu^0, Cu^{1+} or Cu^{2+}) in the initial stages of oxidation, and precise thermodynamic driving forces (e.g., temperature, oxygen pressure) delineating the crossover among different reaction stages and oxidation states of Cu are poorly known. With the use of AP-XPS, we monitor the full reaction pathway of the oxidation of Cu(100) from the initial-stage oxygen chemisorption to the subsequent bulk oxide formation. By increasing oxygen pressure in a stepwise way from $pO_2=1\times10^{-7}$ Torr to 1 Torr, we map the range of pO_2 required for the crossover between the different reaction stages starting from oxygen chemisorption induced surface restructuring to the formation of Cu_2O and then to CuO. In conjunction of the XPS, coordinated Auger electron spectroscopy (AES) measurements allow for unambiguously determining the chemical states of Cu in the different stages of oxidation.

2. EXPERIMENTAL DETAILS

The ambient-pressure photoelectron experiments were performed at CFN AP-PES endstation at the IOS beamline of the National Synchrotron Light Source II (NSLS-II), Brookhaven National Laboratory. The AP-XPS endstation is equipped with a main chamber with the base pressure $< 5\times10^{-9}$ Torr, a SPECS Phoibos NAP 150 hemispherical analyzer, and an Ar-ion sputtering gun. The AP-XPS system has several differential pumping stages between the sample compartment (main chamber) and the hemispherical analyzer, which result in different gas pressures in these two chambers, that is, maintaining UHV conditions (lower than 1×10^{-7} Torr) in the analyzer when the pressure in the main

chamber is a few Torr. Photo-emitted electrons leave the high-pressure sample compartment through a small aperture in a conical piece into the differentially pumped transfer lenses system towards the electron energy analyzer, allowing for continuously acquiring XPS spectra at pressures of up to ~ 5 Torr. The photon energy range of the beamline is from 250 eV to 2000 eV, which covers the O 1s, C 1s and Cu 2p core levels relevant for the current work. Real-time monitoring of the oxidation process was performed by acquiring spectra of O 1s, Cu 2p and Cu $L_3M_{45}M_{45}$ in-situ in the presence of gas at photon energy of 1150 eV. This photon energy provides sufficient penetration depth for detecting the oxide layering. Meanwhile, this photon energy also allows for resolving Cu $2p_{1/2}$ (L_2) level that has the binding energies of 952.3 eV[17].

The Cu(100) single crystal (purchased from Princeton Scientific Corp, purity = 99.9999%) is a top-hat shaped disc (1 mm thick and 8 mm in diameter), cut to within 0.1° to the (100) crystallographic orientation and polished to a mirror finish. The crystal was heated via a ceramic button heater, and its temperature was monitored with a type-K thermocouple. The Cu(100) surface was cleaned by repeated cycles of Ar^+ bombardment (5×10^{-5} Torr of Ar gas, 1 μA cm^{-2}, 1.0 keV, 20 min) at room temperature followed by annealing at 600 °C (UHV, 10 min) until no O and C spectra could be detected by XPS. A separate system equipped with the capabilities of surface structure and morphology characterization, that is, low-energy electron diffraction (LEED) and low-energy electron microscopy (LEEM) imaging, was used to check the surface quality of the Cu(100) surface prepared using the same sputtering and annealing procedure as the AP-XPS experiments. The as-cleaned surface showed sharp diffraction spots of the (1×1) structure and appeared as flat terraces separated by atomic steps.

High-purity oxygen gas (purity = 99.9999%) was directly introduced to the sample compartment through a variable-pressure leak valve to oxidize the freshly cleaned Cu(100) surface at

350°C with the stepwise increase of oxygen pressure from $pO_2=1\times10^{-7}$ to 1 Torr. Continuous collection of the spectra of the O 1s, Cu 2p, and Cu $L_3M_{45}M_{45}$ region was performed at the take-off angle of 70° from the surface normal for surface sensitivity for 30 min or longer time of oxygen exposure at each pO_2. The intensities of the spectra between different oxygen pressures were not quantitatively compared because the photoelectron counts can be affected by gas-phase molecules. Instead, quantification of the surface oxygen coverage and oxide thickness was made with normalizing the intensity of the O 1s with the Cu 2p acquired at the same pO_2. Spectral analysis was performed using the Gaussian/Lorentz product formula and Voigt lines with the Shirley background correction. The energy scale was calibrated using the standard binding energy (BE) of metallic Cu 2p 3/2 at 932.6 eV[18,19].

3. RESULTS AND DISCUSSION

3.1 Progressive Oxidation Stages from Oxygen Chemisorption to Bulk Oxide Formation

Fig. 1 shows the spectra obtained from the Cu 2p, O 1s and Cu $L_3M_{45}M_{45}$ during the exposure of the Cu(100) at 350°C to O_2 with the stepwise increase of pO_2 from $pO_2=1\times10^{-7}$ to 1 Torr. The oxygen exposure at each pO_2 lasts 30 min or longer to ensure that a saturated state is reached before a higher pO_2 is applied. As shown in Fig. 1(a), the shape and position of the Cu 2p3/2 core level peak (BE = 932.6 eV) obtained with the stepwise increase of oxygen pressure from $pO_2=1\times10^{-7}$ to 1×10^{-3} Torr remain the same as that from the freshly cleaned Cu(100) under UHV, indicating that Cu remains its metallic state after the O_2 exposure. This is also confirmed by the Cu $L_3M_{45}M_{45}$ spectra shown in Fig. 1(b), where the profile and peak position located at 918.6 eV remain the same as the these from the Cu(100) under UHV and are characteristic for metallic Cu. There are no noticeable changes in the Cu 2p3/2 spectra after the further pressure increase from $pO_2=1\times10^{-3}$ Torr to 1×10^{-2} Torr, however, the Cu

$L_3M_{45}M_{45}$ spectra shift toward the lower kinetic energy side with the peak located at 916.9 eV, which is the characteristic of Cu^+, indicating that the Cu is oxidized to Cu_2O at $pO_2=1\times10^{-2}$ Torr. The XPS Cu 2p cannot be used to differentiate between Cu^0 and Cu^{1+} because their binding energies are too close (i.e., BE=932.6 eV for Cu^0 and BE=932.4 eV for Cu^+)[18,20] while the Cu $L_3M_{45}M_{45}$ allows for unambiguously distinguishing Cu^0 and Cu^{1+}, as shown in Fig. 1(b).

The subsequent oxygen pressure increase from $pO_2=1\times10^{-2}$ to 1×10^{-1} Torr does not induce noticeable changes in the profile and peak position for both Cu 2p and Cu $L_3M_{45}M_{45}$ after ~ 30 min of oxygen exposure at $pO_2=1\times10^{-1}$ Torr, indicating that the oxide still remains the Cu_2O phase within this pressure range. The oxygen pressure is then increased from $pO_2=1\times10^{-1}$ Torr to 1 Torr, resulting in the peak shift of Cu 2p spectra to BE=933.5 eV with shake-up satellites between 938 eV and 945 eV (Fig. 1(a)), a characteristic feature for Cu^{2+}. This indicates that the surface Cu_2O is further oxidized to CuO at $pO_2=1$ Torr. The CuO formation is also confirmed with the Cu $L_3M_{45}M_{45}$ in Fig. 1(b), which shows the characteristic Cu $L_3M_{45}M_{45}$ kinetic energy of 918.0 eV for CuO.

The oxidation pathway identified from the combined Cu 2p and Cu $L_3M_{45}M_{45}$ spectra is also consistent with the measured XPS O 1s spectra, as illustrated in Fig. 1(c). There is no detectable intensity in the O 1s region under the UHV condition. Exposure at $pO_2=1\times10^{-7}$ Torr results in appreciable intensity in the O 1s core level, indicating the oxygen uptake by chemisorption at the Cu(100) surface. Stepwise increase in oxygen pressure from $pO_2=1\times10^{-7}$ Torr to 1×10^{-3} Torr brings stronger intensity to the O 1s spectra but does not induce noticeable changes in the peak position, confirming that the higher pO_2 allows for building up more chemisorbed oxygen on the surface but is not sufficient for bulk oxide formation. This is in line with the coordinated Cu 2p and Cu $L_3M_{45}M_{45}$ measurements (Figs. 1(a, b)) showing that the Cu(100) remains its metallic state within the range of

oxygen pressure from $pO_2=1\times10^{-7}$ Torr to 1×10^{-3} Torr. With the further increase to $pO_2=1\times10^{-2}$ Torr, the O 1s spectra shifts to the higher energy by 0.5 eV with the peak centered at BE=530.4 eV, which corresponds to the Cu_2O formation. Increasing the oxygen pressure to $pO_2=1\times10^{-1}$ Torr does not induce changes to the O 1s spectra in the peak position, and the further increase in pO_2 to 1 Torr results in the shift of the O 1s peak to BE = 529.7eV, corroborating well with the changes in the Cu 2p and Cu $L_3M_{45}M_{45}$ spectra induced by the oxidation of Cu_2O to CuO at pO_2=1 Torr. It should be mentioned that the O 1s peak intensity drops at $pO_2 > 1\times10^{-3}$ Torr because of the loss of photoelectron counts due to the significant presence of gas molecules in the chamber resulting in inelastic scattering. The combined Cu 2p, Cu $L_3M_{45}M_{45}$ and O 1s measurements shown above are mutually consistent and delineate the range of pO_2 for the progression of the different oxidation stages for the Cu(100) oxidation at 350°C: accumulative oxygen chemisorption takes place from $pO_2=1\times10^{-7}$ Torr to 1×10^{-3} Torr; crossover from oxygen chemisorption to Cu_2O growth occurs within $pO_2=1\times10^{-2}$ Torr and 1×10^{-1} Torr; Cu_2O is further oxidized to CuO upon increasing pO_2 to 1 Torr. In the following sections, we elucidate the mechanism for each stage of the surface oxidation with more detailed XPS measurements.

3.2 Stages of Oxygen Chemisorption

Cu(100) develops two superstructures upon oxygen chemisorption: a disordered p(2×2) structure, in which oxygen atoms are adsorbed in the four-fold hollow sites of Cu(100) and the surface coverage of oxygen is less than 0.3 ML[15,21]; increase in oxygen adsorption results in its transition to the $(2\sqrt{2}\times\sqrt{2})R45^\circ-\mathrm{O}$ MR reconstruction, in which oxygen atoms adsorb to every other four-fold hollow sites and every fourth <100> row of the uppermost Cu atoms is missing[22,23]. It should be noted that each oxygen atom in the MR reconstruction is coordinated with three Cu atoms due to the missing

of Cu atom rows. While the atomic structure of these two surface reconstructions has been determined from post-mortem analyses using atomically resolved probes such as scanning tunneling microscopy (STM) imaging of the reconstructed surfaces formed by dosing a small amount of oxygen in UHV conditions and at elevated temperature and then cooling to the room temperature for characterization, the mechanism and kinetics of the oxygen chemisorption induced reconstruction process are not addressed based on the post-mortem tools. A recent study using AP-XPS monitored the transition from the p(2×2) to MR reconstruction[13] . Here we mainly focus on the kinetic aspect of the oxygen chemisorption process.

Fig. 2(a) illustrates representative spectra of O 1s obtained as a function of time for the oxygen exposure with the stepwise increase in pO_2. The freshly cleaned Cu(100) surface remains the metallic state without detecting noticeable O 1s intensity and is then exposed to $pO_2=1\times10^{-7}$ Torr resulting in appreciable intensity in the O 1s region initially centered at BE=529.3 eV and then stabilized at 529.9 eV. Once no further changes in the peak intensity and position are detected, the oxygen pressure is then increased. Each time after reaching a saturated peak intensity, a stepwise increase in pO_2 is applied and a larger intensity is again observed after ~ 20 min of oxygen exposure. This shows that additional oxygen chemisorption is possible on the oxygenated surface with the saturated O 1s intensities established at lower pressure and a new saturated O 1s intensity is observed in each pressure regime. This stepwise increase in the saturated intensity of the O 1s spectra continues until reaching $pO_2=1\times10^{-4}$ Torr, within which the intensity of the O 1s spectra remains essentially constant, irrespective of the prolonged oxygen exposure and further increase in oxygen pressure to $pO_2=1\times10^{-3}$ Torr. Therefore, this saturated O 1s intensity corresponds to the fully developed $(2\sqrt{2}\times\sqrt{2})R45°$ −O MR reconstruction that has the maximum oxygen surface coverage of 0.5 ML prior to the onset of the bulk oxide formation.

Fig. 2(b) shows more detail about the O 1s spectra from the oxygen exposure at $pO_2=1\times10^{-7}$ Torr. For the initial oxygen exposure (1 min), the O 1s can be deconvoluted into two peaks at BE=529.3 eV and 529.9 eV, which can be assigned to the oxygen in the p(2×2) and MR reconstruction, respectively[13]. Upon the increased oxygen surface coverage from the oxygen exposure at this oxygen pressure, the MR peak intensity increases concomitantly with the decrease in the p(2×2) peak intensity. The correlated evolution in the intensity of the two peaks suggests that the p(2×2) reconstruction serves as a precursor to the MR reconstruction. After ~ 20 min of the oxygen exposure, the p(2×2) reconstruction is barely visible due to the strong peak intensity associated with the MR reconstruction.

Fig. 2(c) corresponds to the evolution of the integrated intensities of the O 1s spectra as a function of oxygen exposure time and oxygen pressure. The intensity of the O 1s spectra in Fig. 2(b) can be used to determine the oxygen surface coverage by normalizing the O 1s intensity with the Cu 2p intensity using the oxygen surface coverage of 0.5 ML for the MR reconstruction at $pO_2=1\times10^{-3}$ Torr as the reference. It can be seen that the oxygen surface coverage in $pO_2=1\times10^{-7}$ Torr saturates at ~0.28 ML, which corresponds to a mixture of p(2×2) and MR reconstruction. The oxygen surface coverage gradually increases to a relatively stable level at each pO_2 and reaches the saturated coverage of 0.5 ML at $pO_2=1\times10^{-4}$ Torr. This corresponds to the completion of the p(2×2)→$(2\sqrt{2}\times\sqrt{2})R45°$ surface phase transformation. Further oxygen exposure at $pO_2=1\times10^{-4}$ Torr and 1×10^{-3} Torr does not result in more oxygen uptake, indicating that the $(2\sqrt{2}\times\sqrt{2})R45°$ reconstructed surface is inert toward further oxidation to the bulk oxide phase that requires a higher pO_2, as described later in sections 3.3 and 3.4.

The temporal evolution of the oxygen surface coverage as a function of pO_2 shown in Fig. 2(b) can be described adequately by the Langmuir isotherm for dissociative gas adsorption. By assuming that the oxygen gas behaves as an ideal gas (this is typically the case for low gas pressures as examined

here for oxygen chemisorption) under the isothermal condition, the dependence of the equilibrium oxygen surface coverage on pO_2 follows

$$\theta = \frac{\sqrt{b(pO_2)}}{1+\sqrt{b(pO_2)}}, \qquad (1)$$

where b is a constant that depends on temperature only. The Langmuir isotherm predicts that the equilibrium oxygen coverage increases with increasing gas pressure for a constant temperature. Fig. 3(a) shows the equilibrium oxygen coverage θ (determined in Fig. 2(b)) plotted as a function of pO_2. The plot of the linearization of the Langmuir is shown in Fig. 3(b), where we can see that the oxygen coverage can be fitted well with the Langmuir isotherm of Eq. (1) as a function of pO_2.

The dissociative oxygen adsorption is further confirmed by analyzing the kinetic data of the oxygen coverage. As shown in Fig. 2(b), we observe an initial rapid increase of the oxygen coverage, followed by a drastic reduction in the oxygen uptake approaching to the equilibrium oxygen coverage at each pO_2. This is because the number of empty sites available for oxygen adsorption decreases as the surface is gradually covered by oxygen. New adsorption takes place at the remaining empty sites with the increase in pO_2. The experimentally measured oxygen adsorption kinetics can be analyzed using the pseudo-second-order model[24]

$$\frac{d(\theta_t)}{dt} = k(\theta_e - \theta_t)^2 , \qquad (2)$$

where θ_t is the oxygen coverage at time t and θ_e the equilibrium oxygen coverage at each pO_2, k is the rate constant of adsorption. Integrating this for the boundary conditions t = 0 to t = t and $\theta_t = 0$ to $\theta_t = \theta_t$, Eq. (2) can be rearranged to obtain

$$\frac{t}{\theta_t} = \frac{1}{k\theta_e{}^2} + \frac{1}{\theta_e}t . \qquad (3)$$

Fig. 3(b) shows the plot of the linearized form of the pseudo-second order model in Eq. (3) with the experimental data obtained from different pO_2 and given in Fig. 2(b). The highly significant linear

relationship between the oxygen coverage, $\frac{t}{\theta_t}$, and t shown in Fig.3(c) indicates that the oxygen chemisorption on the Cu(100) surface is a pseudo-second-order process. The good fitting of the pseudo-second-order equation also indicates that the adsorption for molecular oxygen by the Cu surface is chemisorptive involving valency forces through the sharing of electrons between copper and oxygen atoms[25]. It should be mentioned that the oxygen chemisorption is a complex multistep process that involves surface impingement of gaseous molecules, surface diffusion and surface reaction, and the pseudo-second kinetics is a lump sum of the physical and chemical processes.

3.3 Progression to the Cu_2O Formation

Further increase in oxygen pressure from pO_2 = 1×10^{-3} Torr to 1×10^{-2} Torr results in the nucleation and growth of Cu_2O on the Cu(100)-$(2\sqrt{2}\times\sqrt{2})R45°$ reconstructed surface. Auger Cu $L_3M_{45}M_{45}$ provides the fingerprint to monitor this transition by distinguishing the valence state of Cu^0 and Cu^{1+}. Fig. 4(a) illustrates the temporal evolution of the Cu $L_3M_{45}M_{45}$ spectra during the oxygen exposure at pO_2 = 1×10^{-2} Torr and 1×10^{-1} Torr. In addition to the main peak at 918.6 eV of metallic Cu (i.e., Cu^0), an extra peak gradually shows up at the lower kinetic energy of 916.9 eV corresponding to the valence state of Cu^{1+}. This indicates that the MR reconstructed surface is gradually oxidized to Cu_2O with the co-existence of metallic Cu and Cu_2O. The metallic Cu peak weakens and disappears after ~20 min of oxygen exposure at pO_2=0.1 Torr, indicating that the entire surface is covered by a Cu_2O layer with its thickness greater than the XPS detection depth of about 3 nm estimated by $d = 3\lambda\sin\alpha$,[26] where λ and α are the inelastic mean-free path for photoelectrons and the take-off angle, respectively.

Quantitative kinetic analysis of the oxygen uptake for the $(2\sqrt{2}\times\sqrt{2})R45°$ →Cu_2O transformation can be performed using the temporal evolution of the O 1s spectra. As shown in Fig.

4(b), the surface is initially covered with chemisorbed oxygen with BE=529.9 eV. A gradual shift of the O 1s spectra towards the higher binding energy is observed with the oxygen exposure at $pO_2 = 1\times10^{-2}$ Torr. The O 1s spectra can be deconvoluted into two components, one corresponding to the chemisorbed O with BE=529.9 eV and the other peak located at BE=530.4 eV corresponding to lattice O in Cu_2O. The coexistence of chemisorbed O and lattice O suggests that the $(2\sqrt{2}\times\sqrt{2})R45°$→$Cu_2O$ transformation is controlled by the nucleation and growth of Cu_2O islands on the MR reconstructed surface, where the observed chemisorbed O peak is associated with the $(2\sqrt{2}\times\sqrt{2})R45°$ areas while the lattice O peak is associated with Cu_2O islands. This corroborates well with in-situ electron microscopy observations showing that the early-stage oxidation of Cu involves the nucleation and growth of Cu_2O islands[27–35]. The intensity evolution of these two peaks shown in Fig. 4(b) is directly related to the consumption of the $(2\sqrt{2}\times\sqrt{2})R45°$ regions by the nucleation, growth, and coalescence of Cu_2O islands.

Fig. 4(c) shows the temporal evolution in the peak intensity of chemisorbed O associated with $(2\sqrt{2}\times\sqrt{2})R45°$ areas and lattice O in Cu_2O during the oxygen exposure at $pO_2=1\times10^{-2}$ Torr and 0.1 Torr, respectively. In the initial period, the lattice O intensity increases quickly, followed by slow growth to a relatively saturated level. By contrast, the chemisorbed O drops quickly and then slowly becomes completely attenuated. This indicates that the $(2\sqrt{2}\times\sqrt{2})R45°$ surface areas are completely consumed and the entire surface is now covered by a continuous Cu_2O layer, for which the surface oxidation rate slows down drastically. As can be seen in Fig. 4(c), further increase in oxygen pressure to pO_2=0.1 Torr results in significant additional oxide growth to a new saturated thickness. Surprisingly, the lattice O intensity drops slightly after the longer time of oxygen exposure at pO_2=0.1 Torr. This can

be caused by the effect of non-planar oxide growth induced surface roughening because the emission intensity of photoelectrons from a rough surface decreases with the increase in surface roughness[36].

3.4 Final Progression to the CuO Formation

Further increase in oxygen pressure from pO_2 = 0.1 Torr to 1 Torr results in the oxidation of Cu_2O to CuO. Fig. 5 shows the evolution of the Cu 2p, O 1s and Cu $L_3M_{45}M_{45}$ spectra acquired at pO_2=1 Torr. As shown in Fig. 5(a), the Cu 2p spectra shift quickly toward the higher binding energy side with the characteristic shake-up satellites for CuO. When the Cu^{2+} appears, the simultaneous growth of the satellite peaks and decrease in the Cu $2p_{3/2}$ peak result in a significant decrease in the F parameter (the ratio of the $Cu2p_{3/2}$ peak intensity to the shake-up satellites intensity, referred to $F=I(Cu2p_{3/2})/I(\text{shake-up})$[37]). Hence, the F parameter is highly sensitive to surface Cu^{1+}. The F value for the Cu 2p spectra for the oxygen exposure at 12 min is 2.72, which is greater than 2.46 at 25 min. It indicates the presence of a Cu_2O phase in the early minutes at pO_2=1 Torr in spite of strong satellites intensity. As shown in Fig. 5(b), the Cu 2p peak of the Cu_2O component diminishes completely after 23 min of the oxygen exposure at pO_2 = 1 Torr. This indicates that the surface is quickly covered with a relatively thick CuO layer, for which the emission intensity of photoelectrons from the inner Cu_2O layer is completely attenuated. The fast CuO formation can be also confirmed from the evolution Cu $L_3M_{45}M_{45}$ spectra in Fig. 5(c), which show that the peak intensity associated with the Cu_2O component diminishes quickly and disappears completely after ~ 20 min of the oxygen exposure at pO_2=1 Torr.

Copper forms two thermodynamically stable oxides, CuO and Cu_2O, on the reaction with oxygen. As shown above, the Cu_2O phase is stable and does not further oxidize to CuO after ~ 47 min of oxygen exposure at pO_2=0.1 Torr. The CuO formation becomes favorable upon the oxygen pressure

increase to pO_2=1 Torr, which results in CuO growth on top of the Cu_2O layer with the concomitant formation of the CuO/Cu_2O interface. Such oxide layering is governed by the oxygen gas equilibrium conditions with the stability of CuO > Cu_2O at the higher oxygen pressure. The layered oxide growth is driven by chemical potential gradient across the oxide layers due to many orders of magnitude in oxygen gas pressure between O_2/CuO, CuO/Cu_2O and Cu_2O/Cu interfaces. Within $pO_2=1\times10^{-2}$ Torr and 0.1 Torr, Cu_2O forms on the Cu(100)-$\left(2\sqrt{2}\times\sqrt{2}\right)R45°$ reconstructed surface. With the increase in pO_2 to 1 Torr, CuO formation becomes thermodynamically more favorable, thus CuO growth takes place on the Cu_2O layer. The thickening of the CuO layer results in a significant drop in the oxygen pressure at the buried CuO/Cu_2O interface, for which the Cu_2O phase becomes more favorable. Therefore, the inner portion of the oxygen-richer phase (i.e., CuO layer) undergoes decomposition to form more oxide of the Cu_2O layer at the Cu_2O/CuO interface. Such CuO/Cu_2O bilayer oxide growth produces Cu vacancies and electron holes at the O_2/CuO and CuO/Cu_2O interfaces, which migrate through the CuO and Cu_2O layers, being annihilated finally at the Cu_2O/Cu interface[16].

Fig. 6 summarizes the evolution of the O 1s intensity that delineates the range of oxygen pressures required for the progressive propagation of the different oxidation stages toward the bulk oxide formation and Fig. 7 schematically illustrates the different oxidation stages. At $pO_2=1\times10^{-7}$ Torr, oxygen chemisorption takes place to form the p(2×2) reconstruction. Upon increasing oxygen exposure time and with increasing pO_2 to 1×10^{-6} Torr, the p(2×2) transforms to the $\left(2\sqrt{2}\times\sqrt{2}\right)R45°$ reconstruction. Stepwise increase in pO_2 to 1×10^{-5} Torr and then to 1×10^{-4} Torr results in the completion of the p(2×2)→$\left(2\sqrt{2}\times\sqrt{2}\right)R45°$ transformation. The $\left(2\sqrt{2}\times\sqrt{2}\right)R45°$ surface is inert toward further oxidation until the oxygen pressure is increased to 1×10^{-2} Torr, at which the surface is oxidized to Cu_2O by the nucleation and growth of Cu_2O islands. Increasing pO_2 to 0.1 Torr results in significant Cu_2O

growth but without further oxidation to CuO. The CuO formation becomes more favorable at the higher pressure of pO_2 =1 Torr, at which the surface oxidation occurs via the CuO/Cu_2O bilayer growth. It is noted from Fig. 6 that the gradually decreased O 1s intensity at pO_2 =0.1 Torr is related to the oxide growth induced surface roughening effect while the initial large drop in the O 1s intensity at pO_2 =1 Torr is caused by the loss of photoelectron counts due to the significant presence of gas molecules at the higher pressure.

It is worth mentioning that the phase transformation sequence identified here is from the oxidation experiments at 350°C. This temperature provides sufficient reaction kinetics for using in-situ APS to monitor the different stages of the oxidation. Meanwhile, the experiments at this temperature also facilitate direct comparison with extensive data in the literature from intermediate temperature range for Cu oxidation[16, 38–44]. A change in oxidation temperature may change the oxygen pressure for establishing equilibrium between the different phases as identified in our in-situ AP-XPS experiments. Qualitatively speaking, a higher temperature results in a larger oxygen pressure for phase equilibria, as shown by surface X-ray diffraction[45,46].

It is informative by also comparing our results with the known phase diagrams of the Cu-O system. Under the condition of T=350°C and $pO_2=1\times10^{-6}$ Torr, the formation of either Cu_2O or CuO is expected to set in based on the Cu-O bulk phase diagrams[47,48] . However, our AP-XPS results showed that the Cu(100) surface only develops the missing-row reconstruction (i.e., chemisorbed oxygen) without Cu_2O or CuO formation at T=350°C with the oxygen pressure up to $pO_2=1\times10^{-6}$ Torr. This indicates that the surface oxidation does not proceed beyond the oxygen chemisorbed phase, despite the favorable thermodynamic conditions for bulk oxide formation. Our results corroborate well with other *in situ* measurements of the Cu oxidation. For instance, the Cu-O phase diagram determined by

Eastman and co-workers using synchrotron x-ray scattering revealed a striking difference in behavior compared to the bulk phase diagram during the initial oxidation of Cu(001), showing that the surface only underwent the p(2×2) to MR reconstruction transition with the oxygen pressure ranging from 1×10^{-10} Torr to 1×10^{-4} Torr for the temperature from 27°C to 723°C without Cu_2O or CuO formation[45] and the Cu-Cu_2O phase boundary shifted several orders-of-magnitude upwards in oxygen pressure for the formation of Cu_2O islands[46] compared to the prediction from the bulk thermodynamics or ab initio atomistic thermodynamics calculations[49,50] . Similarly, using *in situ* x-ray diffraction, Lundgren *et al.* monitored the oxidation processes of Pd(001) from oxygen surface chemisorption to the growth of PdO phase and found that the formation of PdO requires a surprising significantly larger oxygen pressure than that predicted by first-principles atomistic thermodynamics[51]. Such a large oxygen pressure required for bulk oxide formation is unexpected by thermodynamics and suggests the existence of a significant kinetic barrier for transforming chemisorbed oxygen into the lattice oxygen in a bulk oxide. It was shown recently that this kinetic hindrance toward the bulk oxide formation can be related to the nucleation of 3D oxide islands for which the nucleation rate is negligibly small until the oxygen pressure reaches a critical value at which the nucleation rate suddenly and dramatically increases and this critical oxygen pressure is many orders of magnitude larger than the equilibrium oxygen pressure predicted from the bulk thermodynamics[52,53].

4. CONCLUSIONS

We have monitored the full reaction pathway of the oxidation of Cu(100) at 350°C. The exposure of a clean Cu(100) surface to $pO_2=1\times10^{-7}$ Torr results in the oxygen chemisorption with the p(2×2) reconstruction that transforms to the $\left(2\sqrt{2}\times\sqrt{2}\right)R45°$ MR restructuring upon increased oxygen

coverage. The MR reconstructed surface is inert toward further oxidation with increasing the oxygen pressure up to 1×10^{-3} Torr. Further increase in pO_2 to 1×10^{-2} Torr results in the nucleation and growth of Cu_2O islands by consuming the $(2\sqrt{2}\times\sqrt{2})R45°$ regions. Significant Cu_2O growth is observed by increasing pO_2 to 0.1 Torr without detectable CuO signal. the CuO formation becomes more favorable after pO_2=1 Torr is reached, at which the surface oxidation occurs via the CuO/Cu_2O bilayer growth. The full reaction pathway of the transition towards a stable oxide has hitherto rarely been addressed for the oxidation of many metals. With the use of AP-XPS techniques, we have mapped the range of pO_2 required for the crossover between the different reaction stages starting from oxygen chemisorption induced surface restructuring to the formation of Cu_2O and then to CuO. The results reported in this work may serve as a guide for the choice of optimal oxidation conditions to control the phase, atomic structure, and stoichiometry of the surface oxide, which has practical significance for many applications such as heterogeneous catalysis.

Acknowledgements:

This work was supported by the U.S. Department of Energy, Office of Basic Energy Sciences, Division of Materials Sciences and Engineering under Award No. DE-SC0001135. This research used resources of the Center for Functional Nanomaterials and the 23-ID-2 (IOS) beamline at the National Synchrotron

Light Source II, which are U.S. DOE Office of Science Facilities, at Brookhaven National Laboratory under Contract No. DE-SC0012704.

References

(1) Lawless, K. R. The Oxidation of Metals. *Rep. Prog. Phys.* **1974**, *37* (2), 231.

(2) Li, L.; Mi, X.; Shi, Y.; Zhou, G. Precursor to the Onset of the Bulk Oxidation of Cu(100). *Phys. Rev. Lett.* **2012**, *108* (17), 176101.

(3) Besenbacher, F.; Nørskov, J. K. Oxygen Chemisorption on Metal Surfaces: General Trends for Cu, Ni and Ag. *Prog. Surf. Sci.* **1993**, *44* (1), 5–66.

(4) Salmeron, M.; Schlögl, R. Ambient Pressure Photoelectron Spectroscopy: A New Tool for Surface Science and Nanotechnology. *Surf. Sci. Rep.* **2008**, *63* (4), 169–199.

(5) Frank Ogletree, D.; Bluhm, H.; Hebenstreit, E. D.; Salmeron, M. Photoelectron Spectroscopy under Ambient Pressure and Temperature Conditions. *Nucl. Instrum. Methods Phys. Res. Sect. Accel. Spectrometers Detect. Assoc. Equip.* **2009**, *601* (1), 151–160.

(6) E. Starr, D.; Liu, Z.; Hävecker, M.; Knop-Gericke, A.; Bluhm, H. Investigation of Solid/Vapor Interfaces Using Ambient Pressure X-Ray Photoelectron Spectroscopy. *Chem. Soc. Rev.* **2013**, *42* (13), 5833–5857.

(7) Nagase, K.; Zheng, Y.; Kodama, Y.; Kakuta, J. Dynamic Study of the Oxidation State of Copper in the Course of Carbon Monoxide Oxidation over Powdered CuO and Cu_2O. *J. Catal.* **1999**, *187* (1), 123–130.

(8) Naeemi, A.; Sarvari, R.; Meindl, J. D. Performance Comparison between Carbon Nanotube and Copper Interconnects for Gigascale Integration (GSI). *IEEE Electron Device Lett.* **2005**, *26* (2), 84–86.

(9) Lindström, B.; Pettersson, L. J. Hydrogen Generation by Steam Reforming of Methanol over Copper-Based Catalysts for Fuel Cell Applications. *Int. J. Hydrog. Energy* **2001**, *26* (9), 923–933.

(10) Mariño, F.; Boveri, M.; Baronetti, G.; Laborde, M. Hydrogen Production via Catalytic Gasification of Ethanol. A Mechanism Proposal over Copper–Nickel Catalysts. *Int. J. Hydrog. Energy* **2004**, *29* (1), 67–71.

(11) Venkatesan, S. P.; Uday, D. S.; Hemant, B. K.; Goud, K. R. K.; Kumar, G. L.; Kumar, K. P. I.C. Engine Emission Reduction by Copper Oxide Catalytic Converter. *IOP Conf. Ser. Mater. Sci. Eng.* **2017**, *197* (1), 012026.

(12) Chi, H.; Andolina, C. M.; Li, J.; Curnan, M. T.; Saidi, W. A.; Zhou, G.; Yang, J. C.; Veser, G. Dependence of H2 and CO2 Selectivity on Cu Oxidation State during Partial Oxidation of Methanol on Cu/ZnO. *Appl. Catal. Gen.* **2018**, *556*, 64–72.

(13) Posada-Borbón, A.; Hagman, B.; Schaefer, A.; Zhang, C.; Shipilin, M.; Hellman, A.; Gustafson, J.; Grönbeck, H. Initial Oxidation of Cu(100) Studied by X-Ray Photo-Electron Spectroscopy and Density Functional Theory Calculations. *Surf. Sci.* **2018**, *675*, 64–69.

(14) Kittel, M.; Polcik, M.; Terborg, R.; Hoeft, J.-T.; Baumgärtel, P.; Bradshaw, A. M.; Toomes, R. L.; Kang, J.-H.; Woodruff, D. P.; Pascal, M.; et al. The Structure of Oxygen on Cu(100) at Low and High Coverages. *Surf. Sci.* **2001**, *470* (3), 311–324.

(15) Gattinoni, C.; Michaelides, A. Atomistic Details of Oxide Surfaces and Surface Oxidation: The Example of Copper and Its Oxides. *Surf. Sci. Rep.* **2015**, *70* (3), 424–447.

(16) Yuan, L.; Wang, Y.; Mema, R.; Zhou, G. Driving Force and Growth Mechanism for Spontaneous Oxide Nanowire Formation during the Thermal Oxidation of Metals. *Acta Mater.* **2011**, *59* (6), 2491–2500.
(17) Lebugle, A.; Axelsson, U.; Nyholm, R.; Mårtensson, N. Experimental L and M Core Level Binding Energies for the Metals 22 Ti to 30 Zn. *Phys. Scr.* **1981**, *23* (5A), 825.
(18) Gaarenstroom, S. W.; Winograd, N. Initial and Final State Effects in the ESCA Spectra of Cadmium and Silver Oxides. *J. Chem. Phys.* **1977**, *67* (8), 3500–3506.
(19) Klein, J. C.; Proctor, A.; Hercules, D. M.; Black, J. F. X-Ray Excited Auger Intensity Ratios for Differentiating Copper Compounds. *Anal. Chem.* **1983**, *55* (13), 2055–2059.
(20) Platzman, I.; Brener, R.; Haick, H.; Tannenbaum, R. Oxidation of Polycrystalline Copper Thin Films at Ambient Conditions. *J. Phys. Chem. C* **2008**, *112* (4), 1101–1108.
(21) Fujita, T.; Okawa, Y.; Matsumoto, Y.; Tanaka, K. Phase Boundaries of Nanometer Scale c(2×2)-O Domains on the Cu(100) Surface. *Phys. Rev. B* **1996**, *54* (3), 2167–2174.
(22) Jensen, F.; Besenbacher, F.; Laegsgaard, E.; Stensgaard, I. Dynamics of Oxygen-Induced Reconstruction of Cu(100) Studied by Scanning Tunneling Microscopy. *Phys. Rev. B* **1990**, *42* (14), 9206–9209.
(23) Yata, M.; Rouch, H.; Nakamura, K. Kinetics of Oxygen Surfactant in Cu(001) Homoepitaxial Growth. *Phys. Rev. B* **1997**, *56* (16), 10579–10584.
(24) Ho, Y.-S. Review of Second-Order Models for Adsorption Systems. *J. Hazard. Mater.* **2006**, *136* (3), 681–689.
(25) Ho, Y. S.; McKay, G. Pseudo-Second Order Model for Sorption Processes. *Process Biochem.* **1999**, *34* (5), 451–465.
(26) Briggs, D.; Seah, M. P. *Practical Surface Analysis, Auger and X-Ray Photoelectron Spectroscopy*; Wiley, 1990.
(27) Yang, J. C.; Bharadwaj, M. D.; Zhou, G.; Tropia, L. Surface Kinetics of Copper Oxidation Investigated by In Situ Ultra-High Vacuum Transmission Electron Microscopy. *Microsc. Microanal.* **2001**, *7* (6), 486–493.
(28) Zhou, G.; Yang, J. C. Formation of Quasi-One-Dimensional Cu2O Structures by in Situ Oxidation of Cu(100). *Phys. Rev. Lett.* **2002**, *89* (10), 106101.
(29) Zhou, G.; Yang, J. C. Temperature Effect on the Cu2O Oxide Morphology Created by Oxidation of Cu(0 0 1) as Investigated by in Situ UHV TEM. *Appl. Surf. Sci.* **2003**, *210* (3), 165–170.
(30) Zhou, G.; Yang, J. C. Initial Oxidation Kinetics of Copper (110) Film Investigated by in Situ UHV-TEM. *Surf. Sci.* **2003**, *531* (3), 359–367.
(31) Zhou, G.; Yang, J. C. Temperature Effects on the Growth of Oxide Islands on Cu(110). *Appl. Surf. Sci.* **2004**, *222* (1), 357–364.
(32) Zhou, G.; Yang, J. C. In Situ UHV-TEM Investigation of the Kinetics of Initial Stages of Oxidation on the Roughened Cu(110) Surface. *Surf. Sci.* **2004**, *559* (2), 100–110.
(33) Zhou, G.; Yang, J. C. Initial Oxidation Kinetics of Cu(100), (110), and (111) Thin Films Investigated by in Situ Ultra-High-Vacuum Transmission Electron Microscopy. *J. Mater. Res.* **2005**, *20* (7), 1684–1694.
(34) Zhou, G. W. TEM Investigation of Interfaces during Cuprous Island Growth. *Acta Mater.* **2009**, *57* (15), 4432–4439.
(35) Zhou, G.; Luo, L.; Li, L.; Ciston, J.; Stach, E. A.; Saidi, W. A.; Yang, J. C. In Situ

Atomic-Scale Visualization of Oxide Islanding during Oxidation of Cu Surfaces. *Chem. Commun.* **2013**, *49* (92), 10862–10864.

(36) Gunter, P. L. .; Gijzeman, O. L. .; Niemantsverdriet, J. . Surface Roughness Effects in Quantitative XPS: Magic Angle for Determining Overlayer Thickness. *Appl. Surf. Sci.* **1997**, *115* (4), 342–346.

(37) Svintsitskiy, D. A.; Chupakhin, A. P.; Slavinskaya, E. M.; Stonkus, O. A.; Stadnichenko, A. I.; Koscheev, S. V.; Boronin, A. I. Study of Cupric Oxide Nanopowders as Efficient Catalysts for Low-Temperature CO Oxidation. *J. Mol. Catal. Chem.* **2013**, *368–369*, 95–106.

(38) Mema, R.; Yuan, L.; Du, Q.; Wang, Y.; Zhou, G. Effect of Surface Stresses on CuO Nanowire Growth in the Thermal Oxidation of Copper. *Chem. Phys. Lett.* **2011**, *512* (1), 87–91.

(39) Zhou, G.; Luo, L.; Li, L.; Ciston, J.; Stach, E. A.; Yang, J. C. Step-Edge-Induced Oxide Growth During the Oxidation of Cu Surfaces. *Phys. Rev. Lett.* **2012**, *109* (23), 235502.

(40) Li, L.; Luo, L.; Ciston, J.; Saidi, W. A.; Stach, E. A.; Yang, J. C.; Zhou, G. Surface-Step-Induced Oscillatory Oxide Growth. *Phys. Rev. Lett.* **2014**, *113* (13), 136104.

(41) Li, L.; Cai, N.; Saidi, W.; Zhou, G. Role of Oxygen in Cu(1 1 0) Surface Restructuring in the Vicinity of Step Edges. *Chem. Phys. Lett.* **2014**, *613*, 64–69.

(42) Li, L.; Liu, Q.; Li, J.; Saidi, W. A.; Zhou, G. Kinetic Barriers of the Phase Transition in the Oxygen Chemisorbed Cu(110)-(2 × 1)-O as a Function of Oxygen Coverage. *J. Phys. Chem. C* **2014**, *118* (36), 20858–20866.

(43) Liu, Q.; Li, L.; Cai, N.; Saidi, W. A.; Zhou, G. Oxygen Chemisorption-Induced Surface Phase Transitions on Cu(110). *Surf. Sci.* **2014**, *627*, 75–84.

(44) Yuan, L.; Zhou, G. Enhanced CuO Nanowire Formation by Thermal Oxidation of Roughened Copper. *J. Electrochem. Soc.* **2012**, *159* (4), C205–C209.

(45) Iddir, H.; Fong, D. D.; Zapol, P.; Fuoss, P. H.; Curtiss, L. A.; Zhou, G.-W.; Eastman, J. A. Order-Disorder Phase Transition of the Cu(001) Surface under Equilibrium Oxygen Pressure. *Phys. Rev. B* **2007**, *76* (24), 241404.

(46) Eastman, J. A.; Fuoss, P. H.; Rehn, L. E.; Baldo, P. M.; Zhou, G.-W.; Fong, D. D.; Thompson, L. J. Early-Stage Suppression of Cu (001) Oxidation. *Appl. Phys. Lett.* **2005**, *87* (5), 051914.

(47) Honjo, G. Electron Diffraction Studies on Oxide Films Formed on Metals and Alloys Part 1. Oxidation of Pure Copper. *J. Phys. Soc. Jpn.* **1949**, *4* (4–6), 330–333.

(48) Schmidt-Whitley, R. D.; Martinez-Clemente, M.; Revcolevschi, A. Growth and Microstructural Control of Single Crystal Cuprous Oxide Cu2O. *J. Cryst. Growth* **1974**, *23* (2), 113–120.

(49) Saidi, W. A.; Lee, M.; Li, L.; Zhou, G.; McGaughey, A. J. H. Ab Initio Atomistic Thermodynamics Study of the Early Stages of Cu(100) Oxidation. *Phys. Rev. B* **2012**, *86* (24), 245429.

(50) Duan, X.; Warschkow, O.; Soon, A.; Delley, B.; Stampfl, C. Density Functional Study of Oxygen on Cu(100) and Cu(110) Surfaces. *Phys. Rev. B* **2010**, *81* (7).

(51) Lundgren, E.; Gustafson, J.; Mikkelsen, A.; Andersen, J. N.; Stierle, A.; Dosch, H.; Todorova, M.; Rogal, J.; Reuter, K.; Scheffler, M. Kinetic Hindrance during the Initial Oxidation of Pd(100) at Ambient Pressures. *Phys. Rev. Lett.* **2004**, *92* (4), 046101.

(52) Zhou, G. Nucleation Thermodynamics of Oxide during Metal Oxidation. *Appl. Phys. Lett.* **2009**, *94* (20), 201905.
(53) Zhou, G. Nucleation-Induced Kinetic Hindrance to the Oxide Formation during the Initial Oxidation of Metals. *Phys. Rev. B* **2010**, *81* (19), 195440.

Figure captions:

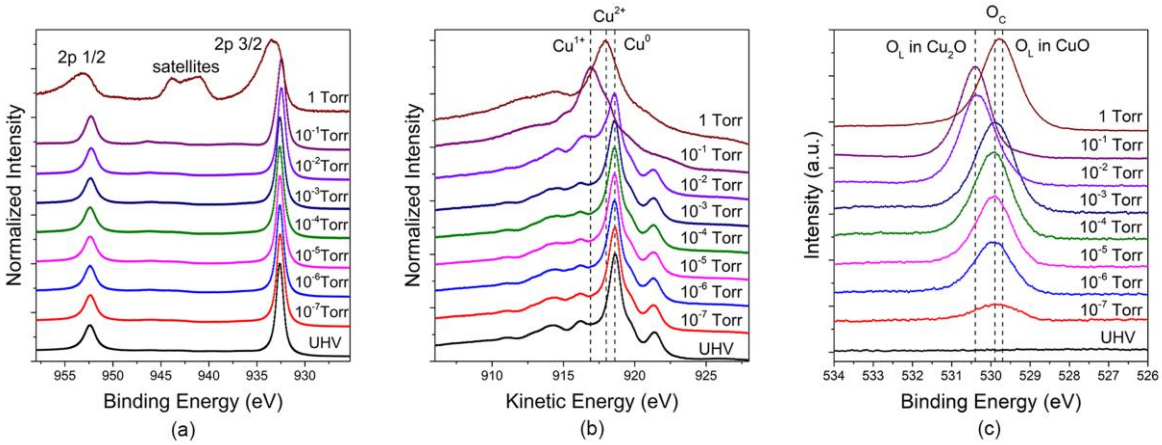

Figure 1: Changes in Cu $2p_{3/2}$ (a), (b) Cu $L_3M_{45}M_{45}$, and O 1s (c) while exposing a clean Cu(100) surface at 350°C to O_2 with stepwise increase of pO_2 from $pO_2=1\times10^{-7}$ to 1 Torr.

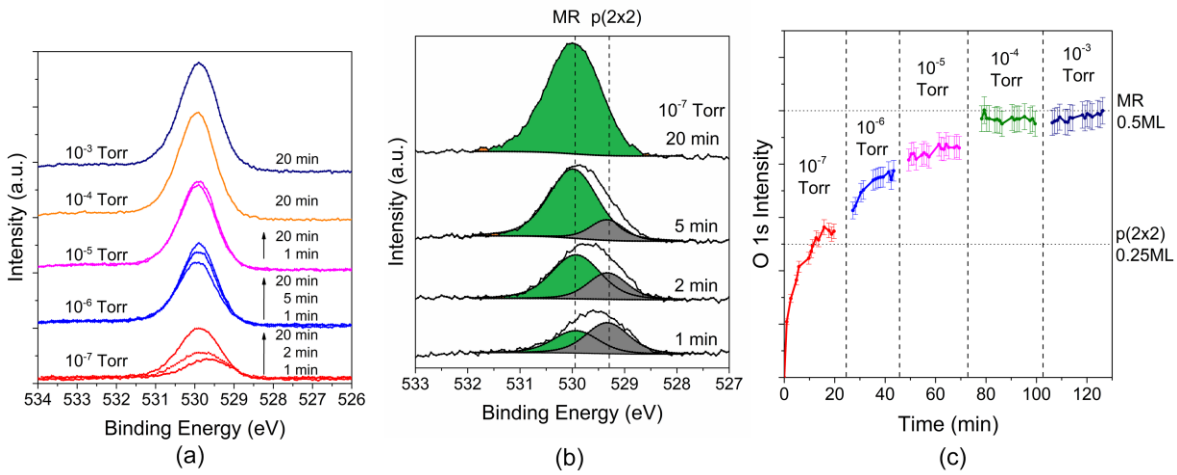

Figure 2: (a) Temporal evolution of the photoemission spectra of the O 1s region upon increasing pO_2. (b) Temporal evolution of the O 1s spectra obtained from the oxygen exposure at $pO_2=1\times10^{-7}$ Torr. (c) Temporal evolution of the integrated intensities of the O 1s spectra. Error bars are added for the slight pressure fluctuations in the chamber.

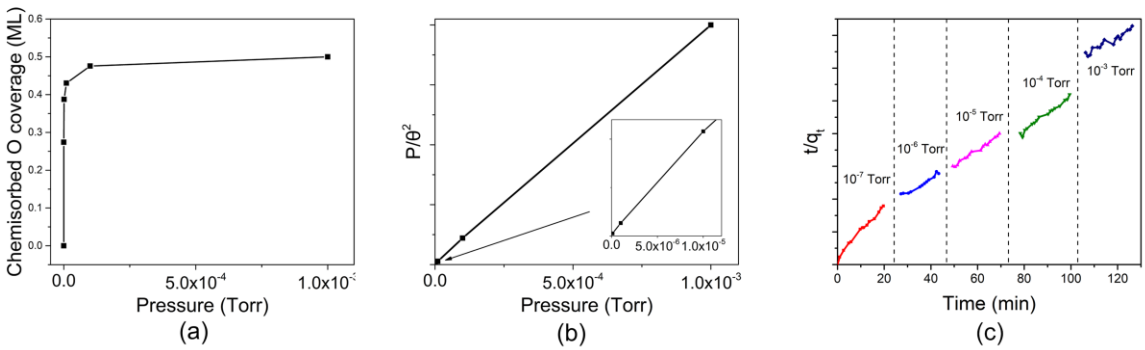

Figure 3: (a) pO_2 dependence of the equilibrium oxygen coverage θ as a function of oxygen gas pressure. (b) Linearization of Langmuir isotherm for chemisorbed O on the Cu(100) surface. The inset shows zoomed-in view of the low oxygen pressure regime ($pO_2<1\times10^{-5}$ Torr). (c) Linearization of the pseudo-second-order equation for chemisorbed O on the Cu(100) surface.

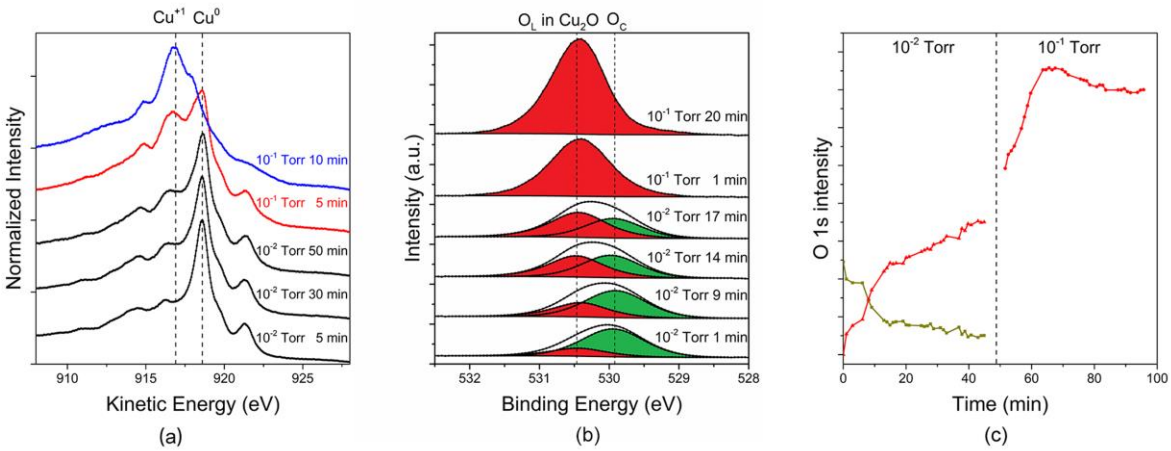

Figure 4: Temporal evolution of Cu $L_3M_{45}M_{45}$ (a), O 1s (b), and integrated intensities of the O 1s region (c) during the exposure of the Cu(100) surface at 350°C to $pO_2=1\times10^{-2}$ and 0.1 Torr, respectively. O_C and O_L in (b) denote chemisorbed O and lattice O in Cu_2O, respectively.

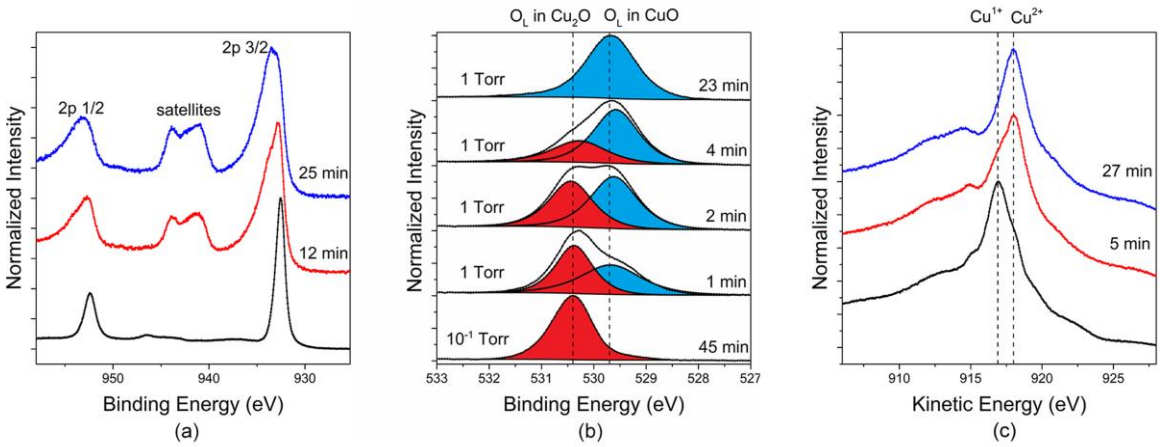

Figure 5: Temporal evolution of Cu 2p spectra (a), O 1s (b), and Cu $L_3M_{45}M_{45}$ (c) during the exposure of the Cu(100) surface at 350°C to pO_2 = 1 Torr. The spectra at the bottom correspond to the oxygen exposure at pO_2 = 0.1 Torr.

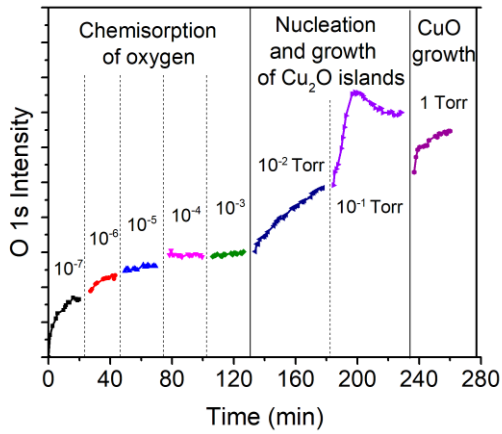

Figure 6: Temporal evolution of the O 1s intensity as a function of oxygen exposure time and oxygen gas pressure for the oxidation of Cu(100) at 350°C. The oxidation starts with a clean Cu(100) surface which is oxidized at $pO_2=1\times10^{-7}$ Torr. A stepwise increase in pO_2 is applied after a relatively saturated O 1s intensity level is reached at each oxygen pressure. The stepwise increase in oxygen pressure results in a corresponding increase of the O 1s intensity until an oxygen pressure of pO_2=0.1 Torr is reached, at which the O 1s intensity initially increases and then decreases due to the Cu_2O growth induced surface roughening. Note that initially large drop in the O 1s intensity with the increase from pO_2=0.1 Torr to

1 Torr is caused by the attenuation of the photoemission signal due to the significant presence of gas molecules at the higher pressure.

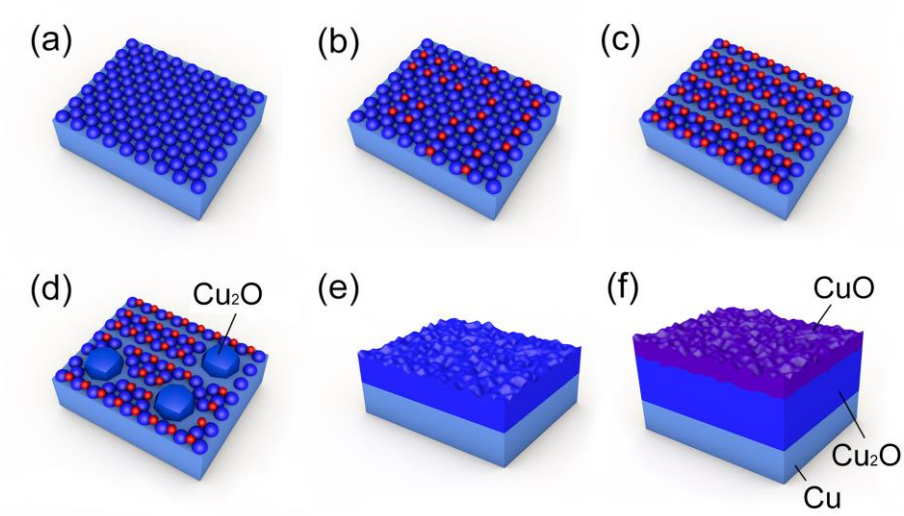

Figure 7: Schematic illustration of the Cu oxidation pathway: (a) clean Cu(100); (b) oxygen chemisorption induced p(2×2) restructuring during the oxygen exposure at $pO_2=1\times10^{-7}$ Torr; (c) $(2\sqrt{2}\times\sqrt{2})R45°$ MR reconstruction with oxygen pressure ranging from $pO_2=1\times10^{-6}$ Torr to 1×10^{-3} Torr; (d) increasing pO_2 to 1×10^{-2} Torr initiates the nucleation and growth of Cu_2O islands by consuming the miss-row reconstructed regions; (e) the increase in pO_2 to 0.1 Torr results in the growth of a continuous Cu_2O layer with a roughened surface, (f) the CuO formation becomes favorable with increasing pO_2 to 1 Torr, at which the surface oxidation occurs via the CuO/Cu_2O bilayer growth, where the inner Cu_2O layer grows at the expense of the CuO at the CuO/Cu_2O interface.

TOC Graphic:

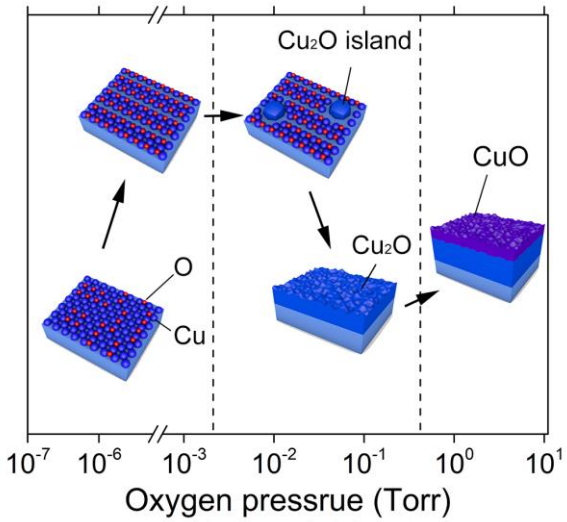
Cu2O island
CuO
Cu2O
O
Cu
10-7
10-6
10-3
10-2
10-1
100
101
Oxygen pressrue (Torr)